NMR Study of the Peierls Transition and the Superconductivity in Quasi One-Dimensional Metallic Compounds: $Nb_{1-x}Ta_xSe_3$

S. Wada and M. Sasakura

College of Liberal Arts, Kobe University, Nada, Kobe 657, Japan

R. Aoki

Department of Physics, Kyushu University 33, Fukuoka 812, Japan

Abstract We describe a NMR study attempting to understand the microscopic mechanism of the antagonistic behavior between the CDW formations and the superconducting transition in Ta-doped $NbSe_3$, both competing for the electronic states near the Fermi surface. The static and dynamic properties of the conduction electrons are probed through their influences on the nuclear spin relaxation time T_1 of ^{93}Nb nuclei. From the characteristic temperature dependence of T_1 in the range 1.4 - 200 K, it is shown that the two CDWs take place within the most conductive column at T_{C1} and within intermediately conductive at T_{C2} of the three inequivalent columns in the unit cell of $NbSe_3$. The Ta-doping in $NbSe_3$ is found to reduce the density of states ρ_F for the two columns, resulting in the suppression of the CDW transition temperatures T_C's. The low temperature conductivity and further the superconductivity occurrence when doped with Ta are analyzed to mainly originate from the remaining less conductive column. A $\omega^{1/2}$ frequency dependence of the experimental T_1 indicates the cohesive motion of conduction electrons to be one dimensional diffusive above the electronic Larmor frequency range for both of the pure and Ta-doped $NbSe_3$. The density of states at low temperatures is also diminished by $\sim 45\,\%$ for an introduction of 5 at.% Ta, which conflicts with the increase of the superconducing transition temperature. It is suggested that the fluctuations of the superconductivity may play an important role for the appearance of the superconducting transition.

I. Introduction

Niobium triselenide, $NbSe_3$, has recently been the subject of intensive studies because of its remarkable physical properties. There are two Peierls transitions which are linked with two independent and incommensurate charge density waves (CDW) at $T_{C1} = 145\,K$ and $T_{C2} = 58\,K$, where the resistivity shows a sharp increase.[1,2] At each transition there is a decrease in the conductivity corresponding to a reduction by $\sim 20\,\%$ of the original carrier content in the first transition and another $\sim 50\,\%$ in the second.[2] The loss of the carriers has been presumed to be due to partial Fermi surface nesting and gapping through the Peierls transitions, leaving a portion ($\sim 30\,\%$) of the Fermi surface open. The reduction of the conductivity is observed in weak electric fields. On the other hand, in strong fields, there is no significant change in the conductivity due to the transitions.[2,3] This non-linear conductivity has been explained by the conduction associated with the CDW motion when the electric energy overcomes the pinning energy.[4] From the magnetization measurements Monceau *et al.*[5] do not see any sign of the superconductivity down to 50 mK under atmospheric pressure.[6] On the other hand, when applied the pressure[5] or doped with impurities such as Ta[6,7] or Zr[8] atoms, the compound becomes a superconductor. The pressure also lowers the temperature at which the resistivity increases, and diminishes the amplitude of the resistivity anomalies. Thus the suppression of the CDW occurrence in the $NbSe_3$ appears to facilitate a break out of the superconductivity as in the most of the low dimensional conductors.

The common behavior of one dimensional (1D) metals towards the Peierls transition originates from the instability of the Fermi surface for a periodic electric field with a wave number $2k_F$.[9] On the other hand, in 3D conductors, the Fermi surface is unstable for the attractive interaction between the electrons resulting in the superconducting transition.[10] Thus it has been suggested that the CDW formation and the superconductivity are antagonistic, both competing for the electronic states near the Fermi surface in a substance. In the $NbSe_3$, nevertheless, microscopic experimental confirmation of how the Fermi surface parameters such as the density of states and the one-dimensionality of the carrier motion are changed when the CDW is suppressed, is not yet clearly established because of its complex crystal structure.

In this paper, we have used the Ta-doping to the $NbSe_3$ to suppress the CDW formations and present a microscopic study on the interplay between the superconductivity and the CDWs. NMR is a measure of the local susceptibilities at the site of the nuclei and has been used as a microscopic probe of the respective amplitudes of the conduction electron wave functions at the various site. The nuclear spin-lattice relaxation time T_1 are related to Fermi surface

parameters and can yield information about the static and dynamic properties of the conduction electrons. The frequency dependence of T_1^{-1} is directly connected with the spectral density of the local spin-fluctuations and provides information about the low dimensionality and degree of coherence of the carrier motion.[11]

There are three inequivalent columns of distorted prismatic cages along the b-axis of the monoclinic unit cell (column I, II, III in Fig. 1) that differ in the surroundings.[12] Each prismatic cage has six Se atoms at the corner and one Nb atom at the center. In our previous paper,[13] a NMR study of the electronic states in the pure $NbSe_3$ has been reported in detail. It was concluded, from the characteristic temperature dependence of T_1 data of ^{93}Nb, the successive CDWs would take place independently in the most conductive column III at T_{C1} and in the intermediately conductive column I at T_{C2}, and the metallic properties at low temperatures are mainly associated with the remaining less conductive column II. Then, in the present paper, we concentrate our attention to possible change of the Fermi surface parameters when doped with Ta atoms in $NbSe_3$.

II. Experimental

$Nb_{1-x}Ta_xSe_3$ ($x = 0,\ 0.005,\ 0.01,\ 0.02,\ 0.05$) were synthesized by direct reaction of Nb, Ta and Se atoms in appropriate proportions and grown by the method described by Meerschaut and Rouxel.[14] For the NMR measurements a large number of the filamentary crystals were mixed with random orientation of the b-axis (powder-like sample).

A pulsed NMR spectrometer operating in the frequency range of 1 - 40 MHz was utilized in the measurements of the ^{93}Nb spin-lattice relaxation time. The ^{93}Nb ($I = \frac{9}{2}$) resonance spectrum in non-cubic symmetry crystal is composed of 9 different lines because of the quadrupole interactions between the nuclear quadrupole moment Q and the electric field gradient q at the site. The severe quadrupole broadening of the resonance spectrum interferes seriously with the T_1 measurement because the recovery curve of the ^{93}Nb magnetization $M(t)$ for the central $\frac{1}{2} \leftrightarrow -\frac{1}{2}$ transition is characterized by five time constants as[15]

$$\frac{[M(\infty) - M(t)]}{M(\infty)} = a_1 e^{-2Wt} + a_2 e^{-12Wt} + a_3 e^{-30Wt} + a_4 e^{-56Wt} + a_5 e^{-90Wt} , \qquad (1)$$

where $2W = T_1^{-1}$ and a_i's are coefficients depending on the initial population of $2I+1$ nuclear spin levels. For the frequency dependence measurement of T_1 at 4.2 K, we applied a saturating comb composed of a few hundred rf pulses before the detection pulses in order to suppress the fast recovery terms ($a_2 \sim a_5$), and we obtained the $2W$ term directly from the experimental recovery curves. For the

temperature dependence measurement of T_1, however, the comb method was not applicable since a comb with a few rf pulses raised the sample temperature by Joule heating. It was also difficult to assign an accurate $2W$ term at high temperature due to the poor signal to noise ratio. Then we recorded full recovery curve of $M(t)$ after single $\pi/2$ rf pulse and assigned a characteristic time $T_1^{(e)}$ at which $[M(\infty) - M(t)]$ has reached 1/e of its initial value. The observed $T_1^{(e)}$ values were normalized to T_1 values at 4.2 K where both the single and the comb saturation method were applicable.

The superconducting transition was detected utilizing the frequency change Δf of a marginal oscillator when the sample in the rf coil entered the Meissner state. Results are shown in Fig. 2, where $\Delta f(T)/\Delta f(0) = 1$ corresponds to a perfect diamagnetism. We defined the superconducting transition temperature T_S at the middle point of the full transition. As can be seen in the figure, the T_S increases rapidly with increasing the Ta-doping up to 5 at.%, while the transition width significantly decreases. The initial rapid increase of T_S is similar to that observed in the pure $NbSe_3$ when applied the pressure.[5]

Typical temperature dependence of the resistivity along the crystal b-axis measured by the four-probe dc method for the samples with $x = 0.005$ and 0.05 was shown in Fig. 3. The resistivity anomalies are considerably smeared out with the Ta-doping, indicative of the suppression of the CDWs.

The temperature dependence of the T_1 was measured at 10.5 MHz for the three samples with $x = 0$, 0.01 and 0.05 in the powder-like form. We obtained resonance spectra of the quadrupole powder-pattern, but each of the satellite lines is not well separated from the other's. The introduction of the Ta atoms broadened each of the lines but hardly affected on the value of the quadrupole coupling constant e^2qQ/h observed for the pure $NbSe_3$.[16] We measured the T_1 at a peak intensity point where the spin echo signal originates mainly from the central transition. Results of the T_1 measurements are shown in Fig. 4 on a log-log scale. Solid lines in the figure show Korringa-like relaxation characteristic of the metals ($T_1T = const.$). The important features of these data are summarized as follows.

a) T_1 follows the $T_1T = const.$ relation in the three (high, intermediate, low) temperature range with different constant values for both of the pure and Ta doped samples. (For 1 at.% Ta sample, the T_1 data at high temperatures was not obtained because of the poor signal intensity.)

b) The characteristic temperature T_C' at which the T_1 begins to deviate and increase from a $T_1T = const.$ relation given in the higher temperature range,

is lowered with increasing the Ta-doping.

c) The T_1T value for each of the three temperature ranges increases with the Ta-doping.

d) In the pure $NbSe_3$, T_1 just below the $T_{C'}$ increases very steeply and exceeds significantly over a extrapolated T_1T value from the lower temperature range. On the other hand, in the Ta-doped $NbSe_3$, the T_1 varies monotonously from the $T_1T = const.$ relation in higher temperature range to that in the successive lower temperature range.

The values of $T_{C1'}$ and $T_{C2'}$ estimated from the data in Fig. 4 are represented in Table 1 with the values of T_S and $(T_1T)^{-1}$ in the high, intermediate and low temperature range.

Fig. 5 is shown of the resonance frequency ω_n dependence of the relaxation rate measured at the low temperature range. Results of $(T_1T)^{-1}$ are plotted as a function of the inverse square root of the ω_n. Straight lines with an almost zero intercept provide the best fit with the experimental data at high frequency range, for both of the pure $NbSe_3$ and $Nb_{.95}Ta_{.05}Se_3$. On the other hand, a level off from the $\omega^{-1/2}$ lines takes place below $\sim$10 MHz.

III. Analysis of T_1 data

As is well known, the nuclear spin relaxation in an ordinary metal is given by the Korringa rate and independent of the resonance frequency. The frequency dependent relaxation in the metallic conductors is a consequence of a finite mean free path l of the conduction electrons characteristic of the low dimensional metals. Thus it has been recognized as an important probe of the diffusive motion of the electrons.[11] For the ^{93}Nb relaxation in the $NbSe_3$, we expect the relaxation rate to be governed by the electron-nuclear hyperfine interactions. In that case,[13]

$$T_1^{-1} = 2\pi\hbar k_B T \gamma_n^2 \rho_F^2 [H_{hf}^2(\mathrm{orb})\, p\, F(\omega_n) + H_{hf}^2(\mathrm{d})\, q\, F(\omega_e)] \quad , \tag{2}$$

where ρ_F is the density of states of the d electrons at the Fermi level E_F, $H_{hf}(\mathrm{d})$ and $H_{hf}(\mathrm{orb})$ are the d core-polarization and orbital hyperfine fields, and p and q are reduction parameters attributed to the symmetry of the d wave functions at E_F. A contribution to the T_1^{-1} from the s contact interaction could be neglected since Nb s band lies even higher in energy above the E_F due to the strong hybridization with Se orbitals.[17,18] The spectral density function $F(\omega)$ reflects the electron motion and depends sensitively on the dimensionality of the diffusive motion. For 1D diffusion,

$$F(\omega) = (2\omega\tau_{//})^{-1/2} \tag{3}$$

where $\tau_{//}^{-1}$ is the intracolumn electron transport relaxation rate arising from the transition across the Fermi sea. The $\omega^{-1/2}$ divergence as $\omega \to 0$ comes from the long wave length part of the momentum transfer ($q \simeq 0$) connecting two points of the Fermi surface. Contribution from $q \simeq 2k_F$ is smaller than that in eq.3 by a factor $(2\omega\tau_{//})^{1/2}$. At low frequency, the 1D diffusion breaks down because of the intercolumn interactions and 2D or 3D behavior is expected. In the two dimension, $F(\omega)$ displays a logarithmic divergence, while in the three dimension it is independent of ω. A cross over between 1D and 2D or 3D regimes occurs at $\omega \simeq \tau_{\perp}^{-1}$, where $\tau_{\perp}^{-1}$ is the intercolumn transport relaxation rate. For a general value of $\omega\tau_{\perp}$, the ω dependence of $F(\omega)$ is expected to be given by[19]

$$F(\omega) \propto \frac{\sqrt{1+\sqrt{1+\omega^2\tau_{\perp}^2}}}{\sqrt{1+\omega^2\tau_{\perp}^2}} , \tag{4}$$

which provides

$$F(\omega) = (1/2\omega\tau_{//})^{1/2} \quad \text{for} \quad \omega\tau_{\perp} >> 1 ,$$

$$F(\omega) = (\tau_{\perp}/\tau_{//})^{1/2} \quad \text{for} \quad \omega\tau_{\perp} << 1 .$$

As can be seen from Fig. 5, the ^{93}Nb relaxation rate T_1^{-1} is proportional to $\omega^{-1/2}$ at high frequency range for both of the pure $NbSe_3$ and $Nb_{.95}Ta_{.05}Se_3$. This result indicates the electron motion to be 1D diffusive at low temperatures. We can rule out any other processes such as paramagnetic impurities which may cause the frequency dependent T_1^{-1}, because the experimental T_1 follows the $T_1T = const.$ relation characteristic of the conduction electron relaxation. The straight lines corresponding to the high frequency range have almost zero intercept which leaves two hypotheses possible since the ^{93}Nb relaxation rate is composed of two contributions depending on the spectral density $F(\omega)$ at ω_n and ω_e frequency, respectively.

a) The 1D diffusive contribution to T_1^{-1} comes from the ω_n range, the contribution from the ω_e being equal to zero: $\tau_{\perp}^{-1} \lesssim \omega_n < \tau_{//}^{-1} < \omega_e$.

b) Only the contribution from the ω_e is 1D diffusive, the contribution from the ω_n being constant (3D diffusive) but considerably small because of the other physical reason: $\omega_n < \tau_{\perp}^{-1} \lesssim \omega_e < \tau_{//}^{-1}$.

For the hypothesis a), a calculated value of the transport relaxation rate for the intracolumn $\tau_{//}^{-1}$ is in the ω_e range and intercolumn $\tau_{\perp}^{-1}$ in the ω_n range.

These are too small to be in a metallic conductor and it turns out not to be the present case of $NbSe_3$. We can thus conclude that the hypothesis b) is physically possible, indicating a dominant core-polarization relaxation in ω_e range. In another words, there should be a considerable reduction of the orbital relaxation. This can be expected only when the d_{z^2} symmetry wave function dominates at the Fermi level, as discussed in ref. 13.

The full lines in Fig. 5 are the best fit of eq. 4, where we took the intercolumn transport relaxation time $\tau_\perp$ being $\simeq 5.7\times10^{-12}$ sec for both of the $NbSe_3$ and $Nb_{.95}Ta_{.05}Se_3$. Thus we may conclude that the intercolumn interaction is not significantly enhanced by the Ta-doping up to 5 at.% and the remnant of the open Fermi surface at low temperatures still be one dimensional in considerable effect. The apparent effect of the Ta doping appears only as a decrease of $(T_1T)^{-1}$ as can be seen in the figure.

Fig. 4 is shown of the temperature dependence of ^{93}Nb relaxation time in the pure $NbSe_3$ and Ta-doped samples with $x = 0.01$ and 0.05.

Detailed analysis of the T_1 data for the pure $NbSe_3$ has been presented in the previous paper.[13] However we'd like to describe it again here because it plays a role of mainstay when considering the data of the temperature dependence of T_1 for the Ta-doped samples.

The experimental T_1 for the pure $NbSe_3$ increases very steeply just below $\simeq 145$ K and $\simeq 50$ K. These temperatures may correspond to the two CDW transition temperatures $T_{C1} = 145$ K and $T_{C2} = 58$ K, respectively.[1,2] Thus the rapid increase of T_1 indicates a growth of the CDW energy gap at the Fermi level. As the temperature decreases a little more, however, the T_1 continues the rapid increase and exceeds significantly over the extrapolated T_1 value from the $T_1T = const.$ in the lower temperature range. The nuclear spin relaxation is attributed to all of the possible momentum transfer within a Fermi sea. Thus, if a partial quenching of the Fermi surface takes place due to a Peierls transition, the T_1 should increase monotonously up to a value determined by the remaining Fermi surface. Therefore the partial quenching mechanism can not solely explain the experimental T_1 behaviors just below the transition temperature and we have to take into consideration the other mechanism for the CDW formations in the $NbSe_3$.

In the monoclinic unit cell of the $NbSe_3$ there are three inequivalent pairs of the trigonal columns.[12] The NMR spectrum observed by Devreux[16] shows the existence of the three inequivalent Nb atom sites with different quadrupole frequencies, indicative of different axial symmetry. Thus in the T_1 measurement one must take into account that the observed spin-echo signal is attributed to ^{93}Nb located at the three sites that differ in the surroundings. The present

characteristic temperature dependence of T_1 in the pure $NbSe_3$ can be understood when one takes into consideration that the observed magnetization recovery curves is composed of three independent ^{93}Nb magnetization recovery curves with different relaxation rates. At high temperature range the $T_1^{(e)}$ is determined by a sum of three different magnetization recovery curves, each of which follows the $T_1T=const.$ relation. When passing through the first transition T_{C1}, a Peierls transition takes place in the most conductive column III and the T_1 in the column increases rapidly due to the CDW energy gap formation at E_F. While, T_1's in the other two columns I and II remain to follow the respective $T_1T=const.$ relations. Thus the $T_1^{(e)}$ in the total recovery curve increases rapidly as the result of the CDW occurrence in the column III. As the temperature is lowered, the T_1 in the column continues the rapid increase and then exceeds a experimental repetitional time t_r of the *rf* pulse sequence ($\pi/2$ — $\pi/2$-π) for the signal averaging. The t_r was set to be t_rT = 40 sec·K. Thus the ^{93}Nb magnetization in the column III begins to saturate and provide negligible contribution to the total recovery curve well below the transition temperature. Consequently, in the intermediate temperature range, the $T_1^{(e)}$ is determined mostly by a sum of the two independent ^{93}Nb magnetization recovery behaviors attributed to the column I and II. In the low temperature range, following above process, the observed T_1 value is expected to correspond directly to the relaxation time in the less conductive column II in which no Peierls transition occurs.

This qualitative analysis seems to be the only and plausible explanation of the characteristic temperature dependence of T_1 in the pure $NbSe_3$. However it should be pointed out here that the temperature dependence of T_1 is measured by the single pulse saturation method and therefore the above analysis is based on the assumption that the coefficients a_i appearing in eq. 1, for the $T_1^{(e)}$ measurement, is independent of the temperature. A possible change of the quadrupole frequency $\Delta\nu_Q$ provides energy shift of the nuclear spin levels and it affects on the value of a_i by a factor $\sim\Delta\nu_Q/\nu_Z$,[15] ν_Z being the nuclear Zeeman frequency. Fortunately the value of ν_Q for the column I which shows any sign of the Peierls transition, is the largest but almost independent of the temperature in the range 4.2 - 300 K.[16] For the other two columns, however, the situation is not clear because it is difficult to know how the coefficients a_i behave at the Peierls transition. Nevertheless we can expect the a_i being almost independent of the temperature since the original values of the quadrupole frequency ν_Q for the column I and III are much smaller than the present experimental Zeemen frequency ν_Z. In veiw of these points we consider the assumption of the temperature independent a_i for the $T_1(e)$ measurements hardly reduces the justification of the qualitative analysis given above.

Thus we may conclude that the nuclear spin relaxation in the pure $NbSe_3$ is performed almost independently within each column. This is consistent with the 1D diffusive motion of the conduction electrons observed at 4.2 K. The two CDWs are considered to be formed independently within the most conductive column III at T_{C1} and intermediately conductive column I at T_{C2}. The metallic properties at low temperatures is considered to originate mainly from the remaining less conductive column II in which no CDW occurs.

As can be seen in Fig. 4, the characteristic temperatures T_{C1}' and T_{C2}' where the T_1T begins to increase are significantly lowered with the Ta-doping. This is indicative of the suppression of the CDW transitions. However we see clearly the two successive T_1T steps even for 5 at.% Ta-doped sample, providing an evidence for the survival of the two independent CDWs. The steep increase of T_1 just below the T_C observed for the pure $NbSe_3$ was smeared out for the Ta-doped samples. This might be caused by a possible distribution of the T_C in the polycrystalline samples. In the $T_1^{(e)}$ measurements, the increase of $T_1^{(e)}T$ is detectable only when the dominant part of the crystals provides the CDW transition. When a significant distribution of T_C exists, even if the T_1 of each crystal increases rapidly just below its own T_C, its contribution to the total magnetization recovery is considered not to be detectable.

Fig. 6 shows a systematic decrease of the ^{93}Nb relaxation rate $(T_1T)^{-1}$ when doped with the Ta atoms for each of the three characteristic temperature range (low, intermediate and high). At the low temperature range, the T_1 was measured by the saturation comb method and therefore the T_1 data are much reliable. The estimated uncertainty is 15 %. The decrease of the $(T_1T)^{-1}$ with the Ta-doping corresponds to a reduction of $\rho_F^2/\sqrt{\tau_{//}}$ appearing in eq. 2.

IV. Discussion

The addition of Ta atoms in $NbSe_3$ appears to produce the superconducting transition as shown in Fig. 2. The superconducting transition temperature T_S is raised steeply with increasing the Ta concentration. On the other hand, the Ta-doping smears the resistivity anomalies originated in the CDW energy gap formation as shown in Fig. 3. From these results of the macroscopic measurements, it can be understood that the CDW formations and the superconductivity are antagonistic but coexist in the Ta-doped $NbSe_3$ at low temperatures. It has been recognized that the introduction of the Ta atoms makes the $NbSe_3$ more three dimensional conductor. Ong and Brill[20] found an anisotropy in the conductivity of $\sigma_{//}/\sigma_{\perp} = 20 \pm 5$, while from the superconducting critical field measurements, Fuller *et al.*[7] have found an anisotropy of 2.39 ± 0.02 in $Nb_{.95}Ta_{.05}Se_3$. These results

seem to suggest the Ta-doped $NbSe_3$ to be less anisotropic than the pure $NbSe_3$.

On the other hand, the results of the present NMR study suggest that microscopic mechanisms of the interplay between the CDWs and the superconductivity in the Ta-doped $NbSe_3$ can't be solely explained by the decline of the one dimensional electronic states. A main difficulty has originated from its complex crystal structure: there are three inequivalent columns in the unit cell that differ in the Se-Se couplings at the base of the distorted prismatic cage[21] and in the surroundings (Fig. 1). From the characteristic temperature dependence of T_1 in the pure $NbSe_3$, we have strongly suggested[13] that a CDW takes place within the most conductive column III with tight $(Se_2)^{2-}$ pairing at T_{C1}, and another CDW within the intermediately conductive I at T_{C2}, independently. The metallic behavior at low temperature is considered to be attributed to the remnant column II which has little Se-Se pairing and is less conductive. This qualitative analysis of the T_1 data is consistent with a band scheme given by Wilson[21] envisaging for the $NbSe_3$.

When the Ta atoms are introduced, the second CDW transition temperature T_{C2}' estimated from the T_1 data is significantly suppressed and the first transition T_{C1}' a little as tabulated in Table 1. On the other hand, a ratio of the relaxation rate below T_{C2}' to above, $(T_1T)^{-1}_{low}/(T_1T)^{-1}_{intermediate}$, is roughly insensitive to the Ta-doping as 0.52 for x = 0, 0.33 for x = 0.01 and 0.53 for x = 0.05. The $(T_1T)^{-1}$ in the low temperature range corresponds to the relaxation rate for the column II, while in the intermediate range the $(T_1T)^{-1}$ is determined by the sum of two independent ^{93}Nb magnetization recovery curves in the column II and I. Then, we tentatively assume here that the observed spin-echo signal for the $T_1^{(e)}$ measurement originates from the central transition of ^{93}Nb in the column II and I in equal proportions and the coefficient a_i in eq. 1 will be the same for the two columns. Thus we can roughly estimate the $(T_1T)^{-1}$ value for the column I, and obtain $(T_1T)^{-1}_{II}/(T_1T)^{-1}_{I} \sim 0.25$ and $\rho_F(II)/\rho_F(I) \sim 0.5$ for both of $NbSe_3$ and $Nb_{.95}Ta_{.05}Se_3$. From the frequency dependence measurement of $(T_1T)^{-1}$ at low temperature, we have made it clear microscopically that the intercolumn coupling hardly increases by the Ta-doping up to 5 at.% and the remnant of the Fermi surface after the two CDW occurrences is expected to be 1D in considerable effect. Thus we may consider that, on the basis of these NMR results, the second CDW at T_{C2}' occurs within the column I and the low temperature conductivity is still attributed mainly to the column II even for the Ta-doped $NbSe_3$. The ratio of the reduction of the carrier concentration at T_{C2}' in the Ta-doped sample doesn't significantly differ from that in the pure $NbSe_3$, in spite of the rapid fall of the second CDW transition temperature T_{C2}'. An apparent effect of the Ta-doping can be found in the decrease of the relaxation rates.

As can be seen in Fig. 6, the $(T_1T)^{-1}$ in each of the three characteristic

temperature range ($T < T_{C2}'$, $T_{C2}' < T < T_{C1}'$, $T_{C1}' < T$) decreases systematically with increasing the Ta atom concentration. The $(T_1T)^{-1}$ is essentially proportional to $\rho_F^2/\sqrt{\tau_{//}}$ as given by eq. 2 . The intracolumn electron transport relaxation time $\tau_{//}$ relates to the electron mean free path l as $\tau_{//} = l/v_F$. When we take into account the impurity scattering, the relaxation time is expressed as

$$\frac{1}{\tau_{//}} = \frac{1}{\tau_{e\text{-}ph}} + \frac{1}{\tau_{imp}} . \qquad (5)$$

Then the introduction of the Ta atoms is considered to reduce the mean free path l and therefore the mean life time $\tau_{//}$. This causes the $(T_1T)^{-1}$ to increase in contrast to the experimentally observed decrease with the Ta-doping. Thus we may consider that the decrease of the $(T_1T)^{-1}$ data provides an estimate of the minimum reduction of the density of states ρ_F at the Fermi level. Then what can be seen in Fig. 6 is a uniform diminution of ρ_F in the three temperature ranges or, roughly speaking, in the three columns. The ρ_F in the low temperature range, which mainly originates from the column II, diminishes by $\sim$45 % at least by 5 at. % Ta-doping.

The suppression of the two Peierls transition temperatures T_{C1} and T_{C2} is considered to be caused by this reduction of ρ_F in the column III and I, respectively, because the reduction of the density of states at the Fermi level diminishes the energy gain of the electron system when the CDW energy gap appears at the Fermi level.

The depression of the resistivity anomalies when doped with Ta atoms is not indicative of a reduction of carrier concentration loss at the CDW transition, but is considered to be a result of the broadening of the CDW transition width. When a CDW takes place in a column and its transition is broad, the decrease of the conductivity in the column is expected to be slow. Then the conductivity in the remnant column without CDW transition may mask the slow decrease of the conductivity in the CDW column well below the CDW transition temperature. The broadening of the CDW transition may originates from the possible distribution of T_C caused by some inhomogeneous distribution of the Ta atoms. Thus the CDW formations in Ta-doped $NbSe_3$ do not have as pronounced effect on the resistivity maxima as they do in the pure $NbSe_3$.

Following above discussion, we may consider that the metallic conduction at low temperatures and further the superconductivity in the Ta-doped samples are mainly attributed to the remnant column II, because the other two columns III and I are quenched in conduction by the CDW energy gap formations below T_{C1} and T_{C2}, respectively. From the frequency dependence measurement of $(T_1T)^{-1}$ at low temperatures, it is shown that the cohesive motion of the conduction electrons re-

mains to be 1D diffusive up to 5 at.% Ta-doping, indicative of the 1D Fermi surface in considerable effect. The immediate result of the Ta-doping appears as the reduction of the density of states at the Fermi level by $\sim 40\,\%$ for $x = 0.01$ and $\sim 45\,\%$ for $x = 0.05$ from that of the pure $NbSe_3$. This significant reduction of the density of states and the remaining of the 1D Fermi surface seem to act against the occurrence of the superconductivity. Thus we must take into consideration other mechanism for the enhancement of the superconductivity.

As can be seen in Fig. 2, the superconducting transition width rapidly decreases with the increase of the Ta concentration, in contrast with the increase of the CDW transition width. The sample of the $NbSe_3$ is considered to be more disordered as the Ta-doping is increased. It results in the increase of the residual resistivity in Fig. 3. Thus, the significant broadening of the superconducting transition width observed with the diminution of the Ta concentration is considered not to be explained by the inhomogeneous distribution of the Ta atoms in the $NbSe_3$.

In the low dimensional systems, it is well known that the fluctuation of the superconductivity is expected to be strongly enhanced and it produces the broadening of the transition width. Fundamental thorems[22,23] demonstrate that no phase transition occurs in one dimension at finite temperatures. Thus we can expect that the fluctuation of the superconductivity plays an important role for the superconductivity occurrence in the $Nb_{1-x}Ta_xSe_3$ compounds. The experimental decrease of the transition width with the Ta-doping would be explained by a suppression of the fluctuation, probably due to the increase of 3D character. This conjecture, however, seems to conflict with the existence of the 1D diffusive motion of the conduction electrons observed in $Nb_{.95}Ta_{.05}Se_3$. This contradiction might be acquiesced when one takes into consideration that the T_1 mesurement reflects the character of a dominant 1D part of the Fermi surface in the column II. If the remaining less 1D part of the Fermi surface carries the superconductivity, we can get out of the dilemma of the dimensionality given above.

Acknowledgement The authors wish to express their sincere thanks to Professor T. Sambongi and M. Ido for kind resistivity measurements of our samples and valuable information.

References

1. J. Chaussy, P. Haen, J. C. Lasjaunias, P. Monceau, G. Waysand, A. Waintal A. Meerschaut, P. Molinié and J. Rouxel, Solid State Commun. 20, 759 (1976).
2. N. P. Ong and P. Monceau, Phys Rev. B16, 3443 (1977).
3. P. Monceau, N. P. Ong, A. Meerschaut and J. Rouxel, Phys. Rev. Lett. 37, 602 (1976).
4. J. Bardeen, *Highly conducting one dimensional solids*, J. T. Devresse eds. (Plenum, New York, 1979) p. 373.
5. P. Monceau, J. Peyard, J. Richard and P. Molinié, Phys. Rev. Lett. 39, 161 (1977).
6. The small and delicate superconductivity below ~ 2.5 K in $NbSe_3$ has been cleared to arise from the crystal boundaries in a polycrystalline sample, by K. Kawabata and M. Ido, to be published in Solid State Commun.
7. W. W. Fuller, P. M. Chaikin and N. P. Ong, Solid State Commun. 30, 689 (1979).
8. K. Kushida, T. Sambongi and M. Ido, J. Phys. Soc. Jpn. 48, 331 (1980).
9. R. E. Peierls, *Quantum Theory of Solids* (Clarendon Press, Oxford).
10. J. Bardeen, L. N. Cooper and J. R. Schrieffer, Phys. Rev. 108, 1175 (1957).
11. S. K. Lyo, Phys. Rev. B 24, 6253 (1981).
12. J. L. Hodeau, M. Marezio, C. Roncan, R. Ayroles, A. Meerschaut, J. Rouxel and P. Monceau, J. Phys. C : *Solid State Phys.* 11, 4117 (1978).
13. S. Wada, R. Aoki and O. Fujita, to be published in J. Phys. F : *Met. Phys.*
14. A. Meerschaut and J. Rouxel, J. Less. Commun. Met. 39, 197 (1975).
15. A. Narath, Phys. Rev. 162, 320 (1967).
16. F. Devreux, J. Phys. (Paris) 43, 1489 (1982).
17. D. W. Bullet, J. Phys. C : *Solid State Phys.* 12, 277 (1979).
18. N. Shima, J. Phys. Soc. Jpn. 52, 578 (1983).
19. G. Soda, D. Jerome, M. Weger, J. M. Fabre and L. Giral, Solid State Commun. 18, 1417 (1976).
20. N. P. Ong and J.W. Brill, Phys. Rev. B 18, 5265 (1978).
21. J. A. Wilson, Phys. Rev. B 19, 6456 (1979).
22. T. M. Rice, Phys. Rev. A 140, 1889 (1965).
23. P. C. Hohenberg, Phys. Rev. 158, 383 (1967).

$Nb_{1-x}Ta_xSe_3$ x		0	0.01	0.05
Super. transi.	T_S (K)	--	0.2 ∿ 0.4	1.5
CDW transi.	T_{C1}'(K)	145	( )	90
	T_{C2}'(K)	50	30	10
$(T_1T)^{-1}$ (sec.K)	$T<T_{C2}'$	0.095	0.034	0.028
	$T_{C2}'<T<T_{C1}'$	0.18	0.13	0.059
	$T_{C1}'<T$	0.25	( )	0.14

Table 1 Experimental superconducting transiton and CDW transition temperature and ^{93}Nb relaxation rates in low, intermediate and high temperature range.

Figure Captions

Fig.1. Plan of the $NbSe_3$ structure with details determined by Hodeau *et al.*[12] *b*-axis into paper.

Fig.2. The superconducting transition of $Nb_{1-x}Ta_xSe_3$ detected by the frequency change of a marginal oscillator.

Fig.3. Temperature dependence of the electric resistivity for $Nb_{.995}Ta_{.005}Se_3$ (——) and $Nb_{.95}Ta_{.05}Se_3$ (---).

Fig.4. Temperature dependence of T_1 of ^{93}Nb in the pure $NbSe_3$ (●), $Nb_{.99}Ta_{.01}Se_3$ (△) and $Nb_{.95}Ta_{.05}Se_3$ (○) at $\omega_n = 10.5$ MHz. Solid lines are the best fit of $T_1T = const.$ relation in the three temperature ranges.

Fig.5. ^{93}Nb relaxation rate $(T_1T)^{-1}$ as a function of the inverse square root of the nuclear Larmor frequency ω_n for the pure $NbSe_3$ (●) and $Nb_{.95}Ta_{.05}Se_3$ (○). at 4.2 K.

Fig.6. ^{93}Nb relaxation rate $(T_1T)^{-1}$ in the $Nb_{1-x}Ta_xSe_3$ in the three temperature ranges: $T < T_{C2}'$, $T_{C2}' < T < T_{C1}'$ and $T_{C1}' < T$.

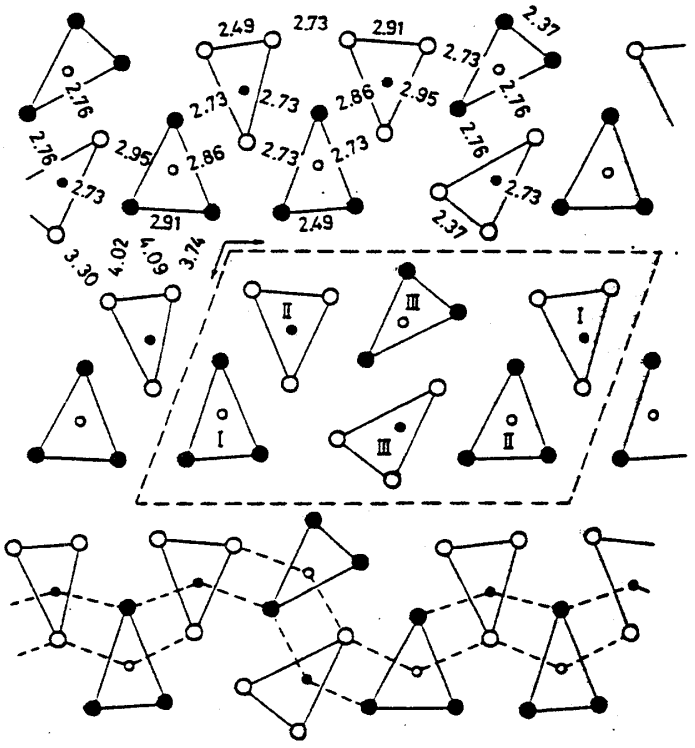

○ Selenium ○ Niobium

Open circle ; y = 1/4

Closed circle; y = 3/4

Fig 1

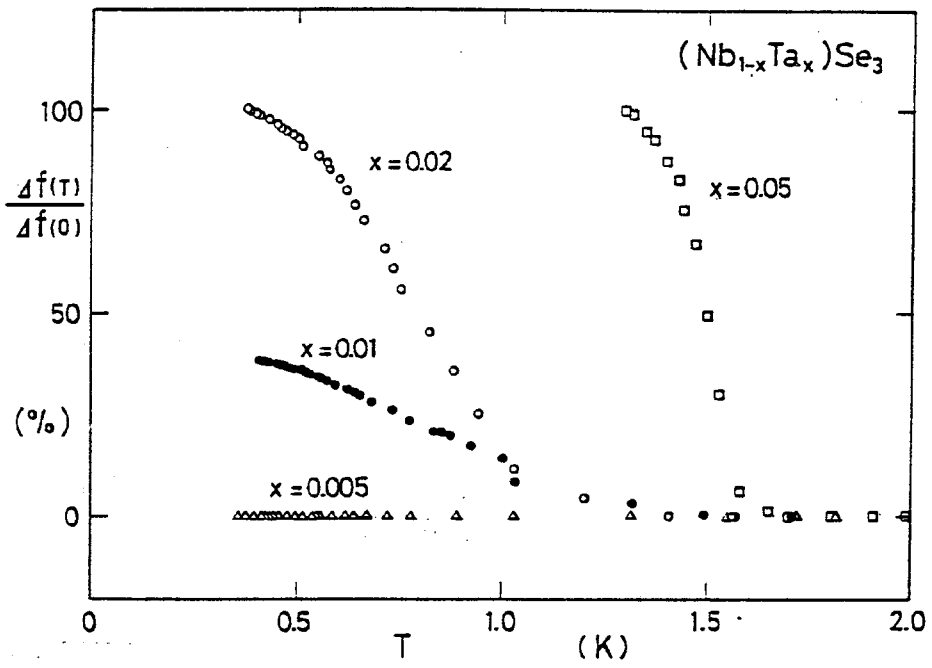
(Nb1-xTax)Se3
100
Δf(T)/Δf(0)
50
(%)
0
x=0.02
x=0.05
x=0.01
x=0.005
0
0.5
1.0
1.5
2.0
T
(K)

Fig 2

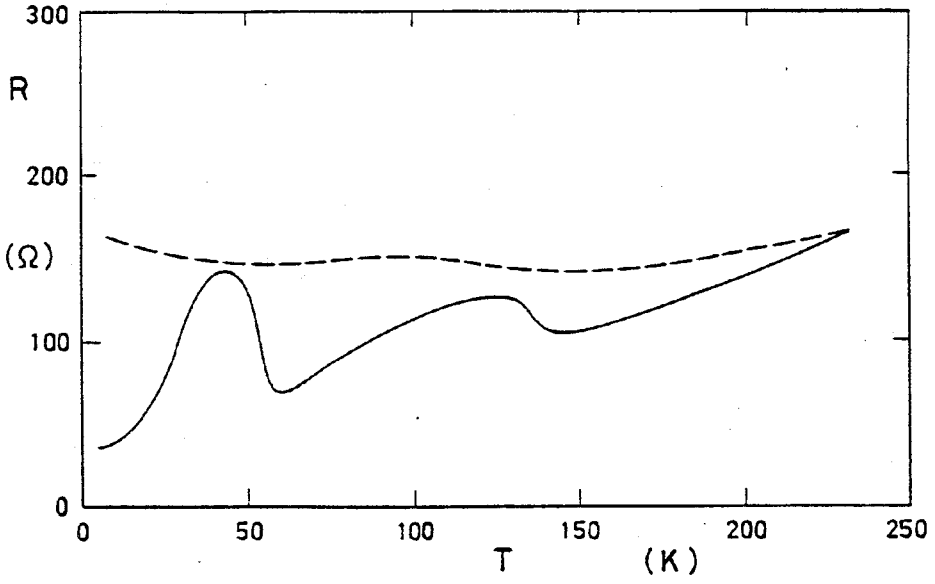
300
R
200
(Ω)
100
0
0
50
100
150
200
250
T
(K)

Fig 3

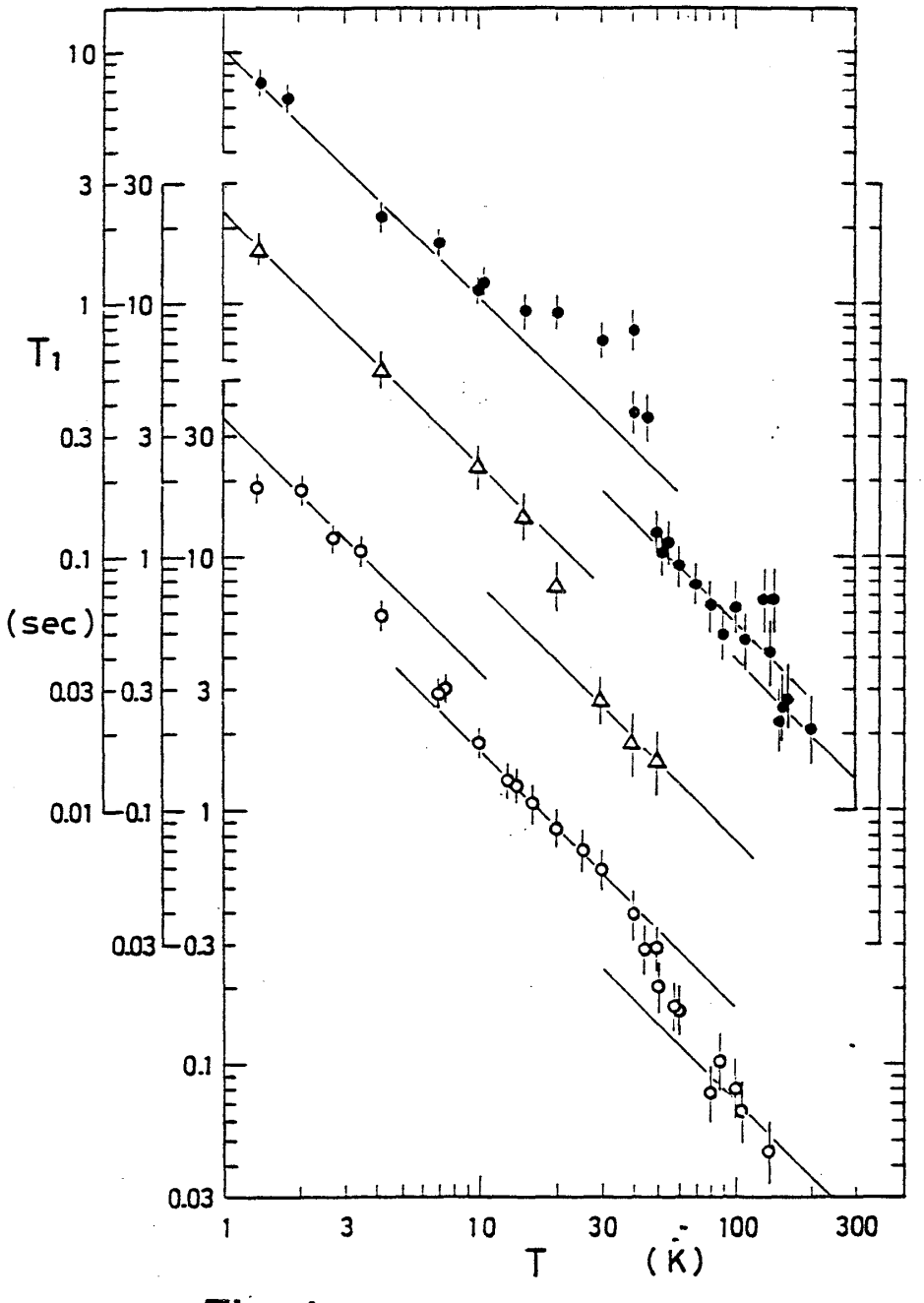

Fig 4

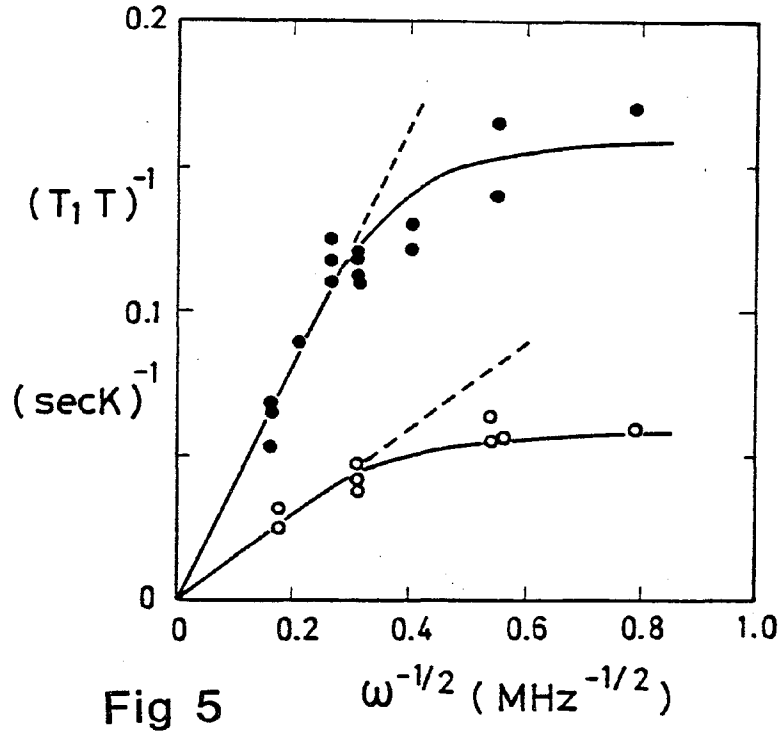
0.2
0.1
0
$(T_1 T)^{-1}$
(secK)$^{-1}$
0
0.2
0.4
0.6
0.8
1.0
$\omega^{-1/2}$ (MHz$^{-1/2}$)

Fig 5

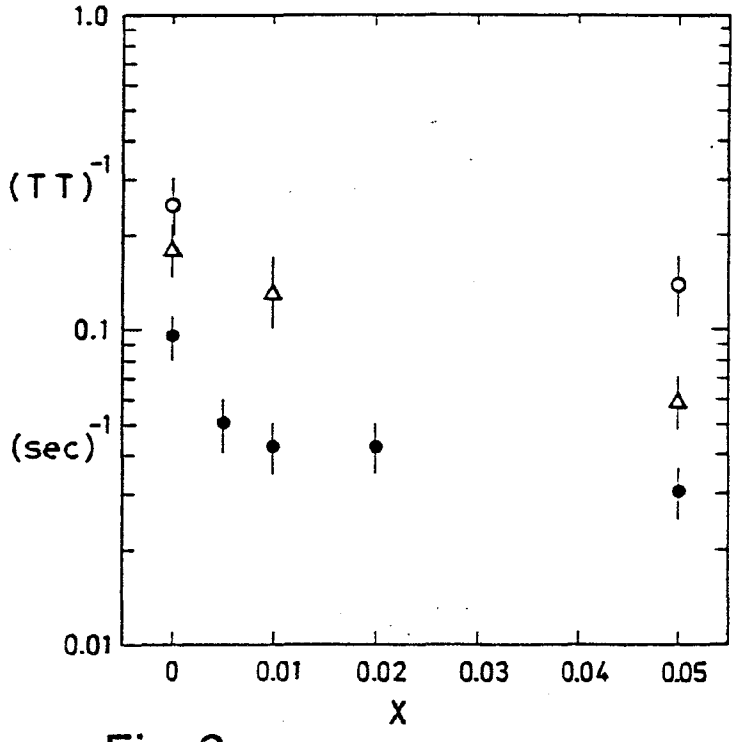
1.0
0.1
0.01
$(T T)^{-1}$
(sec)$^{-1}$
0
0.01
0.02
0.03
0.04
0.05
X

Fig 6